Conformational Polymorphism in Aripiprazole: Preparation, Stability and Structure of Five Modifications

DORIS E. BRAUN,[1] THOMAS GELBRICH,[1] VOLKER KAHLENBERG,[2] RICHARD TESSADRI,[2] JOSEF WIESER,[3] ULRICH J. GRIESSER[1]

[1]Institute of Pharmacy, University of Innsbruck, Innrain 52, 6020 Innsbruck, Austria

[2]Institute of Mineralogy and Petrography, University of Innsbruck, Innrain 52, 6020 Innsbruck, Austria

[3]Sandoz GmbH, Biochemiestrasse 10, 6250 Kundl, Austria

Received 15 June 2008; revised 31 July 2008; accepted 15 August 2008

Published online 13 November 2008 in Wiley InterScience (www.interscience.wiley.com). DOI 10.1002/jps.21574

ABSTRACT: Five phase-pure modifications of the antipsychotic drug aripiprazole were prepared and characterized by thermal analysis, vibrational spectroscopy and X-ray diffractometry. All modifications can be produced from solvents, form I additionally by heating of form X° to ~120°C (solid–solid transformation) and form III by crystallization from the melt. Thermodynamic relationships between the polymorphs were evaluated on the basis of thermochemical data and visualized in a semi-schematic energy/temperature diagram. At least six of the ten polymorphic pairs are enantiotropically and two monotropically related. Form X° is the thermodynamically stable modification at 20°C, form II is stable in a window from about 62–77°C, and form I above 80°C (high-temperature form). Forms III and IV are triclinic ($P\bar{1}$), I and X° are monoclinic ($P2_1$) and form II orthorhombic ($Pna2_1$). Each polymorph exhibits a distinct molecular conformation, and there are two fundamental N–H···O hydrogen bond synthons (catemers and dimers). Hirshfeld surface analysis was employed to display differences in intermolecular short contacts. A high kinetic stability was observed for three metastable polymorphs which can be categorized as suitable candidates for the development of solid dosage forms. © 2008 Wiley-Liss, Inc. and the American Pharmacists Association J Pharm Sci 98:2010–2026, 2009

Keywords: aripiprazole; thermal analysis; conformational polymorphism; IR spectroscopy; Raman spectroscopy; X-ray diffractometry; thermodynamics; Hirshfeld surfaces; single crystal structure

INTRODUCTION

Aripiprazole (7-[4-[4-(2,3-dichlorophenyl)-1-piperazinyl]butoxy]-3,4-dihydro-2(1H)-quinolinone, APZ, Fig. 1), is a second generation antipsychotic drug indicated for the treatment of schizophrenia. The drug is a high-affinity partial agonist at human D_2-receptors and also targets the dopamine autoreceptor, but it has a lower affinity for D_4-receptors. It also shows a partial agonist activity at 5-HT_{1A} receptors and antagonist activity at 5-HT_{2A}. Originally discovered by Otsuka Pharmaceutical Co., the compound was jointly developed by Otsuka and Bristol Myers Squibb and first marketed in the USA in 2002 under the trade name Abilify®.[1]

More than 20 patent applications[2–4,7] claim different APZ solid state forms (polymorphic, solvated, and amorphous forms), mixtures there-

Additional supporting information may be found in the online version of this article.

Correspondence to: Ulrich J. Griesser (Telephone: 43-512-507-5309; Fax: 43-512-507-2939;
E-mail: ulrich.griesser@uibk.ac.at)

Journal of Pharmaceutical Sciences, Vol. 98, 2010–2026 (2009)

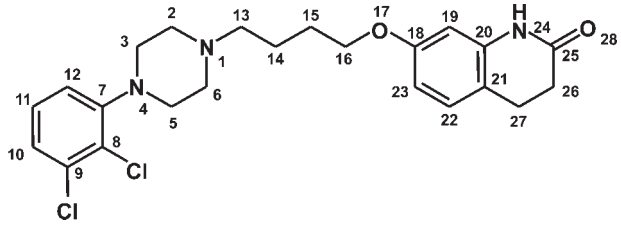

Figure 1. Molecular scheme of APZ ($C_{23}H_{27}Cl_2N_3O_2$, $M_r = 448.39$).

of, as well as the corresponding preparation methods. Some aspects of the monohydrate and of two modifications were already published in 1996 in a conference proceeding.[5] Tessler and Goldberg[6] determined the crystal structures of four solid state forms of APZ, namely an anhydrous form (CSD refcode: MELFIT), the monohydrate (MELFUF), the hemi-ethanol (MELFEP), and mono-methanol solvates (MELFOZ). Furthermore, the lattice parameters of yet another modification were reported in a recent patent application.[7]

The features of its molecular structure (Fig. 1) make APZ very attractive for an investigation of how chemically identical yet conformationally flexible molecules pack in multiple crystal forms. The APZ molecule displays seven freely rotatable bonds (six of them in an aliphatic chain, one connecting the dichlorobenzene ring with the 1,4 substituted piperazine), five hydrogen acceptors, but only one strong H-bond donor. The molecule adopts a strongly elongated shape. Due to its flexibility, one can expect the APZ molecule to adopt different conformations in its various solid state forms (conformational polymorphism[8–10]). However, as we have reported recently,[11] it is also possible that distinct polymorphs of molecules with a high degree of molecular flexibility consist of conformers which are exactly the same. Such cases of "packing polymorphism" of conformationally flexible molecules can occur when the molecules aggregate into a strongly hydrogen bonded unit, which pack in different ways. In contrast to previous reports dealing with the solid state properties of APZ, the aim of our investigation was to gain insight into structure–property relationships of the (nonsolvated) polymorphs and to draw a much clearer picture of this polymorphic system than one can derive from literature data currently available, including patents. Our aim was to characterize, by a variety of analytical techniques, those APZ polymorphs which can be reproducibly prepared so that their structural and thermodynamic features can be assessed. The thermodynamic and kinetic stability of the solid state forms were ascertained by thermal analytical methods such as hot-stage microscopy (HTM) and differential scanning calorimetry (DSC), as well as solvent-mediated transformation studies. FT-IR and FT-Raman spectroscopy, as well as X-ray diffraction methods (powder and single crystal) were applied to evaluate the structural features of the polymorphs. At first, an extensive solid state screening program on APZ was conducted which provided the foundation for all subsequent investigations of this study. Various additional solvate forms were obtained in these experiments, and their properties are the subject of another paper.[12]

EXPERIMENTAL

Materials

A sample of APZ consisting of form III (purity 99.0%) was obtained from Sandoz GmbH, Kundl, Austria. The solvents used in this study were of p.a. quality.

X-Ray Powder Diffractometry (XRPD)

The X-ray powder diffraction patterns (XRPD) were obtained with a Siemens D-5000 diffractometer (Siemens AG, Karlsruhe, Germany) equipped with a theta/theta goniometer, a Cu Kα radiation source, a Göbel mirror (Bruker AXS, Karlsruhe, Germany), a 0.15° Soller slit collimator and a scintillation counter. The patterns were recorded at a tube voltage of 40 kV and a tube current of 35 mA, applying a scan rate of 0.005° 2θ s^{-1} in the angular range of 2–40° 2θ.

Thermal Analysis

Thermomicroscopic investigations (HTM) were carried out with a Reichert Thermovar® polarization microscope (Reichert, Vienna, Austria) equipped with a Kofler hot stage (Reichert). The microphotographs were taken with a digital camera (Olympus DP50, Olympus Optical Co. Ltd, Vienna, Austria). A Kofler hot bench (Reichert) was employed for the preparation of melt film samples (by fusing the substance between a glass slide and a cover slip).

DSC was performed with a DSC 7 (Perkin-Elmer, Norwalk, CT) using the Pyris 2.0 software. Approximately 1–3 ± 0.0005 mg of sample (using a UM3 ultramicrobalance, Mettler, Greifensee, Switzerland) were weighed into Al-pans (25 μL). Dry nitrogen was used as purge gas (purge: 20 mL/min). Temperature calibration was performed with pure benzophenone (m.p. 48.0°C) and caffeine (m.p. 236.2°C), and the enthalpy calibration was performed with indium (purity 99.999%, m.p. 156.6°C, heat of fusion 28.45 J/g). The errors of the stated temperature and enthalpy values (Tab. 1) are calculated at 95% confidence intervals (c.i.) based on at least five measurements.

Spectroscopy

Fourier transform infrared (FTIR) spectra were recorded with a Bruker IFS 25 spectrometer (Bruker Analytische Messtechnik GmbH, Ettlingen, Germany) connected to a Bruker IR microscope I (15x-Cassegrain-objective). The samples were prepared on ZnSe-disks and measured in transmission mode (spectral range 4000–600 cm^{-1}, resolution 4 cm^{-1}, 64 interferograms per spectrum). Raman spectra were measured with a Bruker RFS 100 Raman-spectrometer (Bruker Analytische Messtechnik GmbH), equipped with a Nd:YAG Laser (1064 nm) as the excitation source and a liquid-nitrogen-cooled, high sensitivity Ge-detector. The sample was placed into aluminum sample holders, and spectra were recorded with a laser power of 200 mW (128 scans per spectrum) and a resolution of 2 cm^{-1} (spectral range 4000–30 cm^{-1}).

Solvent Mediated Transformation Studies (SMT)

These experiments were carried out by suspending the solid in a solvent using a glass cylinder, a magnetic stirrer and a thermostated oil or water bath. The suspensions were stirred (900 r.p.m.) either at a constant temperature or by applying several heating cycles (details on the temperature ranges are stated in the Results and Discussion Section).

Table 1. Physicochemical Data for APZ Polymorphs

Modification	I	II	III	IV	X°
T_{fus} [°C]					
TM (equilibrium)	148.5	143	139	135	—
DSC (onset) ± 95% c.i.	149.1 ± 0.1	143.1 ± 0.2	139.2 ± 0.2	134.9 ± 0.2	—
$\Delta_{fus}H$ [kJ/mol] ± 95% c.i.	38.36 ± 0.15	41.51 ± 0.08	39.97 ± 0.17	40.76 ± 0.18	45.1[a]
T_{trs} [°C]					
Experimental (SMT)	I/II: ~65–75	II/X°: ~62	—	—	X°/I: ~77
Calculated[b] [°C]		II/I: 91	III/I: 39	IV/III 37; IV/I: 38	
$\Delta_{trs}H$ [kJ/mol] to form I	—	3.1[c]	1.6[c]	2.4[c]	6.16 ± 0.03[d] 6.73 ± 0.02[e]
Order of thermodynamic stability at 0 K (and presumably at 25°C)	*e*	*b*	*d*	*c*	*a* (highest)
Density order at 25°C (see Tab. 2)	*c*	*e*	*d*	*a* (highest)	*b*
Selected IR-bands[13] [cm^{-1}]					
ν NH (cycl. amide)[f]	3206	3181	3194	3196	3194
ν CH_2[f]	2941	2956	2945	2939	2939
ν C=O	1681	1686	1681	1682	1681
ν O–Ar range	1280/1256/1240	1284/1264/1242	1291/1275/1242	1293/1274/1242	1285/1270/1247
n.a.	1194/1163	1202/1170	1199/1174	1197/1177	1193/1169
ν O–CH_2 range	1045	1047	1045/1032	1044/1031	1049

T_{fus}, melting point; T_{trs}, transition temperature; $\Delta_{fus}H$, enthalpy of fusion; $\Delta_{trs}H$, transition enthalpy; c.i., confidence interval; n.a., not assigned.

[a] Calculated: sum of $\Delta_{fus}H_I$ and $\Delta_{trs}H_{X°\text{-}I}$.

[b] Calculated according to Eq. (2) ($k = 0.003$).

[c] Calculated: difference between $\Delta_{fus}H$ of the individual polymorph and $\Delta_{fus}H_I$.

[d] Freshly crystallized form.

[e] After storage for about 12 months.

[f] Most intensive band.

Single-Crystal X-Ray Diffractometry

The X-ray data were collected at room temperature on a STOE IPDS-II diffractometer using Mo Kα radiation ($\lambda = 0.71073$ Å). The program package WinGX[14] (SIR97[15] and SHELXL97[16]) was used for structure solution and refinement. All the H atom positions were generated in idealized geometries at the parent atoms by a riding model with $U_{iso}(H) = 1.2\ U_{eq}(C/N)$.

The single crystals of form III were of rather low quality and showed hardly any scattering at higher diffraction angles. Therefore, only the 2θ range up to 40° was used for the structure refinement. Additional confirmation of our structure model obtained from this poor quality data set was provided by a comparison with a previous determination of the same structure at low temperature.[6] Despite their shortcomings, the new data proved to be useful for a comparison with the other room temperature structures of the polymorphs.

RESULTS AND DISCUSSION

Our experimental work on APZ suggests the existence of ten crystalline solid state forms (five polymorphs, a monohydrate, four solvates),[12] and the amorphous form.[2] The different crystal forms (polymorphs and solvates) in the numerous patent applications[2–4,7] have been named in various ways. These naming schemes comprise either Roman numerals (I, II, III, ...), Latin capitals B, C, D, or Greek letters (α). However, these terminologies lead to several problems: (a) in some cases different letters or numbers have been assigned to the same crystal form, (b) these naming systems do not distinguish between hydrates/solvates and one-component polymorphs, and (c) individual names have also been allocated for mixtures of different forms. This makes it difficult to get a clear picture of the existing solid state phases of APZ and to denominate them without introducing an entirely new nomenclature. Therefore, we have decided to name the five polymorphs (one-component phases) with Roman numerals following the order of decreasing melting points (Kofler notation, highest melting polymorph is named form I). A fifth modification, which could not be assigned to any of the disclosed forms in patent applications at the time of our study, has been named form X°. This decision was motivated by the fact that we were unable to measure its melting point, as will be discussed in detail below. Form X° is the thermodynamically stable form at room temperature (therefore marked with a superscript zero) and corresponds to "form II" of a recent patent application.[3]

Production and Specification of the Crystal Forms

Form I is the high temperature stable form and can be produced by heating the forms II, III or IV above their melting temperatures and keeping the temperature constant at about 145°C to complete the crystal growth (less than 3 h to avoid thermal decomposition). This works only if small traces (seeds) of form I are present in the investigated sample, which is often the case when the forms are crystallized from solvents. The maximum growth rate of form I from the melt was observed at about 130°C. Heating form X° to about 120°C yields form I via a solid–solid transformation. Form I can also be produced from any given form (or mixture of forms) in a solvent-mediated transformation process above 80°C. In a well stirred suspension with 1-butanol the different polymorphs undergo this transformation within 3 h. Form I is obtained as prismatic plates and melts at 148.5°C.

Form II typically crystallizes concomitantly with other forms. Phase pure form II was obtained by stirring a suspension of APZ in 1-butanol or acetonitrile for at least 1 h, while the temperature was kept between 65 and 75°C. The polymorph occurs as almost needle-like, elongated plates and melts at 143°C. Single crystals of form II were obtained by crystallization from acetonitrile at 70°C.

Form III can be produced in microscopic melt-film preparations from the supercooled melt. On reheating such preparations the nucleation of this form starts spontaneously at about 75°C, and the crystal growth proceeds spherically from the nucleation center. This results in fine-rayed spherulites, whose growth rate accelerates when the temperature is increased (Fig. 2). This form is also obtained by desolvation of the ethanol, methanol and dichloroethane solvates, or the monohydrate.[12] Polymorph III forms irregular plates (when crystallized from 1-butanol) that melt at 139°C. Crystallization experiments showed that form III (single crystals) can also be obtained by crystallization from solvents such as ethyl acetate, 1-butanol, xylene or *n*-hexane, indicating that a nucleation can occur directly in

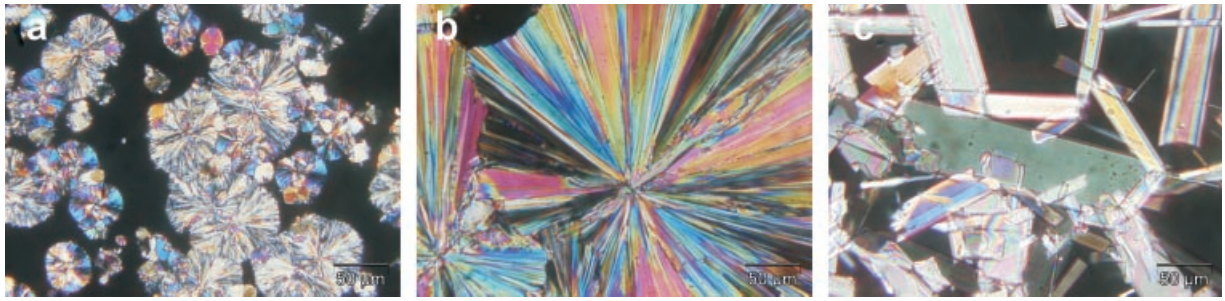

Figure 2. Photomicrographs of (a) spherulites of form III grown at 75°C and (b) crystallized at 120°C from the quench cooled melt; (c) tabular, prismatic crystals of form I obtained by heating form III to 140°C via an inhomogeneous melting process.

these solvents. Our experiments confirm the observation made by Aoki et al.[5] that grinding of form III and subsequent heating above the melting point results in a sample with a higher fraction of form I than the same procedure without grinding.

Form IV can be produced by crystallization from solvents such as toluene and dioxane. Provided that the cooling rate is fast (cooling the hot solution in an ice bath or with 8°C tap water) this form also crystallizes from hot saturated solutions of 2-propanol and acetonitrile. Form IV melts at 135°C and typically crystallizes as rhombohedral plates.

The pure *form X°* can be produced by stirring a suspension of any APZ form in a solvent, which does not form solvent adducts, below 65°C. Suitable solvents are acetone, 1-propanol, 2-propanol, acetonitrile or 1-butanol, and the resulting crystals are tabular prisms.

Thermal Analysis

Hot-Stage Microscopy

In a melt film preparation the supercooled melt of APZ nucleates spontaneously at temperatures above 70°C and grows to fine-rayed spherulites of form III only (Fig. 2a and b). Pure samples of form III melt homogeneously at 139°C. However, if seeds of the high temperature form I are present, an inhomogeneous melting process (melting and simultaneous crystallization of a higher melting phase) occurs and form I grows in the melt until its melting temperature of 148.5°C is attained. Form I grows to highly birefringent tabular prisms (Fig. 2c). During several experiments performed at various temperatures, nucleation from the melt was never observed for any of the other forms (II, IV, or X°). Similar to form III, the polymorphs IV (T_{fus}: 135°C) and II (T_{fus}: 143°C) show inhomogeneous melting to form I, if the respective sample is contaminated with seeds of this form. In contrast to forms II, III and IV, form X° shows a clear solid–solid transition to form I at a temperature of about 120°C.

Differential Scanning Calorimetry

The melting endotherms and enthalpies of fusion of the four phase-pure polymorphs I, II, III, and IV were determined directly at heating rates of 10 K/min. The DSC curves of the five polymorphs are shown in Figure 3, and the determined thermochemical data are listed in Table 1. The highest enthalpy of fusion among these four modifications was measured for form II, which is followed by form IV, form III, and finally form I. All efforts to determine the melting point of form X° failed due to its fast endothermic

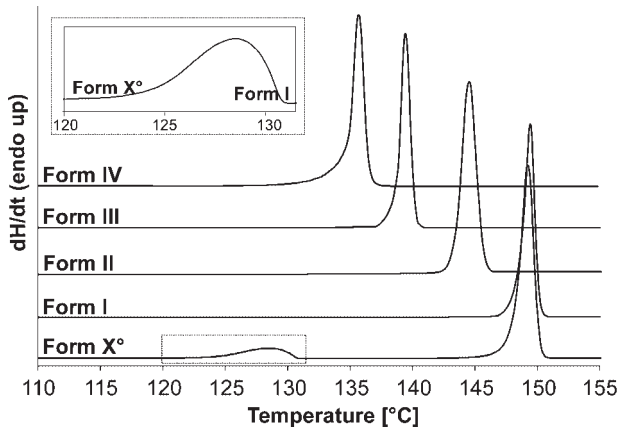

Figure 3. DSC curves of APZ polymorphs (heating rate 10 K/min). The insert shows the endothermic peak of the solid–solid transformation X° to I (enlarged section of the form X° curve).

 DOI 10.1002/jps

phase transition to form I. Even heating rates of 500 K/min (Hyper DSC) were not sufficient to overcome the transition rate kinetics. Freshly crystallized form X° exhibits a heat of transition of $\Delta_{trs}H_{X°\text{-}I} = 6.16 \pm 0.03$ kJ/mol. Due to relaxation phenomena, this value increases on storage by 0.6 kJ/mol to $\Delta_{trs}H_{X°\text{-}I} = 6.73 \pm 0.02$ kJ/mol. This is indeed a particularly high enthalpy change, which is in the range of the enthalpy differences of polymorphs. However, we did not observe a significant change of the melting enthalpies of the other forms (I–IV) on aging.

Thermodynamic and Kinetic Stability of APZ Polymorphs

Relative thermodynamic stabilities of the polymorphic pairs can be determined on the basis of the heat of fusion (HFR) and heat of transition (HTR) rules[17–19] and the obtained melting points. The only missing data point hampering the compilation of the complete set of interrelationships is the melting point of form X°. Five polymorphs ($n = 5$) give $(n-1) \times n/2 = 10$ pairs, which are either monotropically or enantiotropically related. To solve such a complex polymorphic system and to avoid wrong conclusions, it is advisable to construct a semi-schematic energy/temperature diagram (Fig. 4) as described elsewhere.[17–19]

From the HFR rule it is clear that the highest melting form I is enantiotropically related to all the other forms, because it shows the lowest enthalpy of fusion. Although we were not able to measure the melting point of form X°, the observed endothermic phase transition from X° to I proves unequivocally that these forms are enantiotropically related. Thus, we conclude that $T_{fus,X°}$ must be lower than $T_{fus,I}$ (there is a crossing of the free enthalpy curves of X° and I). According to Hess's law of heat summation we can calculate the heat of fusion of form X° ($\Delta_{fus}H_{X°}$) as a sum $\Delta_{fus}H_I + \Delta_{trs}H_{X°\text{-}I}$, which gives 45.1 kJ/mol. The fact that this value represents by far the highest enthalpy of fusion value of all APZ forms is owed to the high heat of transition $\Delta_{trs}H_{X°\text{-}I}$ term. In other words, the enthalpy curve of form X° must run below that of all other forms (Fig. 4) which suggests that form X° is the stable polymorph at absolute zero.

Form III and IV must be enantiotropically related too, since form IV has the lower melting point but a higher heat of fusion than polymorph III. Quite the opposite is true with respect to form

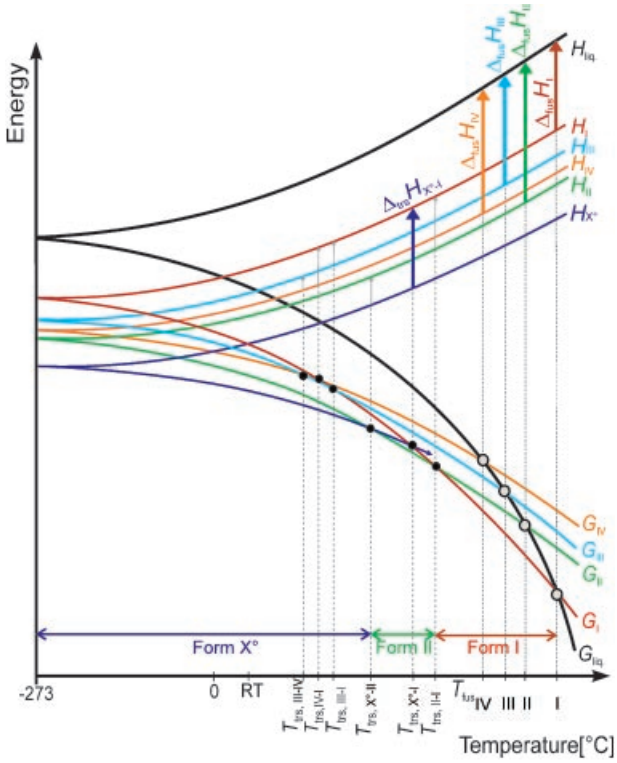

Figure 4. Semi-schematic energy/temperature diagram of APZ polymorphs (I, II, III, IV, and X°). T_{fus}, melting point; G, Gibbs free energy; H, enthalpy; ΔH_f, enthalpy of fusion; T_{trs}, transition point; $\Delta_{trs}H$, transition enthalpy; liq, liquid phase (melt). The bold vertical arrows signify experimentally measured enthalpies, and the horizontal double arrows mark temperature ranges where either polymorph X°, II or I is the thermodynamically stable form.

II, whose melting point and heat of fusion are higher than those of forms III and IV. Therefore, each of the two pairs III/II and IV/II must represent a monotropic relationship. From the course of the G isobars in Figure 4 we conclude that the curves of forms II and X° intersect, which means that these polymorphs are also enantiotropically related. In summary, there are at least six enantiotropic relationships and thus six transition points (marked with black spots in Fig. 4).

Solution-mediated transformation experiments of polymorph mixtures in 1-butanol were performed at various temperatures to assess the thermodynamically stable form within different temperature ranges. Temperature cycles between 10 and 30°C, 40 and 45°C, 50 and 55°C, and 55 and 60°C resulted exclusively in form X°, confirming X° is the stable form at about 60°C and below.

Stirring the suspensions at a constant temperature of 65, 70, or 75°C resulted in form II, whereas form I was obtained at temperatures ≥ 80°C (80, 85, 90, and 100°C). We conclude from these results that form II is the thermodynamically stable form in a narrow temperature window between ~62 and ~77°C. Form I is stable above and form X° is stable below this temperature range, as highlighted in Figure 4. The fact that the enantiotropic transition of form X° to I was the only such transition we were able to measure suggests that all other reversible phase transitions underlie a strong kinetic control.

Not all five polymorphs have the same Z' parameter (see Tab. 2), so that the density rule[17–19] is not a very reliable indicator of the order of their thermodynamic stabilities at absolute zero. This rule is valid for the two triclinic modifications (III and IV), which exhibit only a small difference in their heat of fusion (0.8 kJ/mol), because their conformational differences are small and a common type of strong hydrogen bonds is present (for more detail see below). The density difference of $\Delta d_x = 2.3\%$ is significant and confirms indeed the enantiotropic relationship of these two forms (higher density means lower free energy at absolute zero). The density rule holds also for the five pairs X°/II ($\Delta d_x = 1.9\%$), X°/III ($\Delta d_x = 1.4\%$), X°/I ($\Delta d_x = 0.5\%$), IV/III ($\Delta d_x = 2.3\%$), and IV/I ($\Delta d_x = 1.4\%$), but not for the five others (X°/IV, II/IV, II/III, II/I, and III/I). The highest density difference ($\Delta d_x = 2.8\%$) is encountered for the pair II/IV (Z' not equal). Strikingly, the polymorphic pair where the largest differences with regard to the molecular conformation occur (form I and II,

Table 2. Crystallographic Data for the APZ Polymorphs

Form	I	II	III[a]	IV	X°
Chemical formula	$C_{23}H_{27}Cl_2N_3O_2$	$C_{23}H_{27}Cl_2N_3O_2$	$C_{23}H_{27}Cl_2N_3O_2$	$C_{23}H_{27}Cl_2N_3O_2$	$C_{23}H_{27}Cl_2N_3O_2$
Formula weight	448.38	448.38	448.38	448.38	448.38
Description	Colorless plate	Colorless needles	Colorless plate	Colorless thin rhomb-shaped plate	Colorless plate
Size (mm)	0.5 × 0.4 × 0.11	0.42 × 0.2 × 0.08	0.38 × 0.22 × 0.04	0.4 × 0.12 × 0.02	0.32 × 0.3 × 0.04
Crystal system	Monoclinic	Orthorhombic	Triclinic	Triclinic	Monoclinic
Space group	$P2_1$	$Pna2_1$	$P\bar{1}$	$P\bar{1}$	$P2_1$
T (K)	293 (2)	293 (2)	293 (2)	293 (2)	293 (2)
a (Å)	8.6789 (17)	23.519 (5)	10.220 (2)	8.8180 (5)	8.8669 (18)
b (Å)	7.5683 (15)	12.657 (3)	12.208 (2)	9.0350 (7)	7.7623 (16)
c (Å)	17.381 (4)	7.7560 (16)	18.837 (4)	30.417 (2)	16.485 (3)
α (°)	90.00	90.00	82.28 (3)	88.072 (6)	90.00
β (°)	94.50 (3)	90.00	82.52 (3)	86.550 (6)	93.25 (3)
γ (°)	90.00	90.00	82.88 (3)	73.874 (6)	90.00
V (Å^3)	1138.1 (4)	2308.8 (9)	2295.4 (8)	2244.4 (3)	1132.8 (4)
Z/Z'	2/1	4/1	4/2	4/2	2/1
d_{calc} (Mg/m^3)	1.308	1.290	1.297	1.327	1.315
Reflns. collected	7108	12,836	8044	14,756	7301
Independent reflns.	4001	3480	4112	7445	3791
Observed reflns.	3139	1787	2266	4686	3115
θ Range for data collection	2.35–25.05	1.83–24.76	1.69–20.0	1.34–25.05	2.3–25.05
Range of h, k, l	$-10 < h < 9$ $-9 < k < 9$ $-20 < l < 20$	$-26 < h < 27$ $-14 < k < 14$ $-8 < l < 9$	$-9 < h < 9$ $-11 < k < 11$ $-18 < l < 18$	$-9 < h < 10$ $-10 < k < 10$ $-36 < l < 36$	$-10 < h < 9$ $-9 < k < 8$ $-19 < l < 19$
Data, parameters	4001, 271	3480, 271	4112, 541	7445, 542	3791, 271
Goodness of fit on F^2	1.049	1.100	1.124	1.037	1.074
R_{int}	0.030	0.198	0.301	0.041	0.041
Final R indices [$I > 2\sigma(I)$]	0.0567	0.1003	0.0800	0.0567	0.0445
R indices (all data)	0.1317	0.1472	0.0902	0.1354	0.0921
$\Delta\rho_{max}$, $\Delta\rho_{min}$ (e Å^{-3})	0.37, −0.28	0.24, −0.23	0.19, −0.17	0.19, −0.18	0.19, −0.18

[a]The single crystals of form III were of rather poor quality and showed hardly any scattering at higher diffraction angles. Therefore only the range up to 40° was used for structure refinement.

$Z' = 1$ in both cases) also represents one of the exceptions to the density rule. By contrast, all other exceptions are associated with two unequal Z' parameters. It is apparent that the interrelation between stability, packing efficiency and changes in molecular conformation is very complex, and we have to accept that the density rule, that is, Kitaigorodsky's "dense packing principle"[20] may fail in the case of conformationally flexible molecules such as APZ.

It is possible to estimate the order of the transition points from the obtained melting points and enthalpy of fusion values, a technique that has been already successfully applied to other polymorphic systems.[17,18,21,22] Such calculations, if performed with high-accuracy thermochemical data, are helpful to confirm the graphically obtained order of transition points (from a schematic energy temperature diagram) and also to check of the correctness of the derived relationships between two modifications (monotropism: $T_{trs} > T_{fus}$, enantiotropism: $T_{trs} < T_{fus}$). The calculation is based on the following equation:

$$T_{trs} = \frac{\Delta_{fus}H_2 - \Delta_{fus}H_1 + (C_{p,liq} - C_{p,1})(T_{fus,1} - T_{fus,2})}{\frac{\Delta_{fus}H_2}{T_{fus,2}} - \frac{\Delta_{fus}H_1}{T_{fus,1}} + (C_{p,liq} - C_{p,1})\ln\left(\frac{T_{fus,1}}{T_{fus,2}}\right)} \quad (1)$$

where T_{trs} is the thermodynamic transition point (K), T_{fus} the melting point (K), $\Delta_{fus}H$ the heat of fusion (kJ/mol) and C_p the heat capacity in J/mol/K. The indices 1 and 2 stand for the higher and lower melting form, respectively. Since heat capacities of the melt ($C_{p,liq}$) and the higher melting form ($C_{p,1}$) are usually not available, an empirical correction term $k\,\Delta_{fus}H_1$ can be used for the heat capacity difference $C_{p,liq} - C_{p,1}$. Typical empirical values for k range from 0.001 to 0.007 K^{-1} with an average of $k = 0.003$ K^{-1} according to Yu.[21] Burger and Ramberger[17,18] suggested an upper limit of $k = 0.005$ K^{-1}. With the simplified Eq. (2), assuming $k = 0.003$ K^{-1}, we obtain values of 37, 38, 39, and 91°C for the pairs III/IV, IV/I, III/I, and II/I, respectively (Tab. 1).

$$T_{trs} = \frac{\Delta_{fus}H_2 - \Delta_{fus}H_1 + k\Delta_{fus}H_1(T_{fus,1} - T_{fus,2})}{\frac{\Delta_{fus}H_2}{T_{fus,2}} - \frac{\Delta_{fus}H1}{T_{fus,1}} + k\Delta_{fus}H_1\ln\left(\frac{T_{fus,1}}{T_{fus,2}}\right)} \quad (2)$$

Accordingly, the transition temperatures of the forms III, IV and I pool in a very narrow temperature range slightly above room temperature, but they indicate the same order as can be derived from the course of the free enthalpy curves (Fig. 4). However, the calculated transition temperature of the pair II/I is more than 10°C higher than the value that was determined experimentally from SMT experiments (~77°C). Albeit this deviation is not quite satisfactory, it does not impair the fundamental determination of the complex thermodynamic relationships in this system. The true thermodynamic transition point $T_{trs,X°\text{-}I}$ must be within the temperature range of $T_{trs,X°\text{-}II}$ and $T_{trs,II\text{-}I}$, roughly between 65 and 75°C. This is obvious from the course and the intersection points of the G isobars of form X°, I and II in Figure 4.

A transformation of Eq. (2) gives Eq. (3) [23] which allows the estimation of an unknown melting point from the heat of transition, transition point and melting data (heat and temperature) of the higher melting form. Assuming $T_{trs,X°\text{-}I} = 70$°C and $\Delta_{fus}H_{X°\text{-}I} = 45.1$ kJ/mol (calculated: sum of $\Delta_{fus}H_I$ and $\Delta_{trs}H_{X°\text{-}I}$), a value of $T_{fus,X} = 135.1$°C is obtained. This value is almost equal to the melting point of the lowest melting form IV, which would confirm that form X° and form III are enantiotropically related (heat of fusion rule, melting point of form X° lower than that of form III). However, considering the potential errors of such a calculation, it is not justified to derive a monotropic relationship from the very small difference between the calculated melting point of X° and the experimental m.p. of form IV ($\Delta T = 0.2$°C).

$$T_{fus,2} = \frac{\Delta_{fus}H_2 T_{fus,1} T_{trs}}{T_{fus,1}\Delta_{fus}H_2 + T_{trs}\Delta_{fus}H_1 - T_{fus,1}\Delta_{fus}H_1} \quad (3)$$

It should be stressed that all metastable modifications, except form I, are kinetically highly stable at room temperature. The storage of the pure forms II, III, and IV in glass vessels did not result in any transition to a more stable form, including form X°. By contrast, about 50% of form I transforms under the same conditions to form X° within less than 6 month. Elevated temperatures cause an acceleration of the rate of transition, and it was also observed that mechanically treated samples of form I transform faster.

Infrared and Raman Spectroscopy

The FT-Raman spectra (Fig. 5) of the individual polymorphs show differences in almost the entire spectral range. The most apparent differences can be established in the low-frequency range

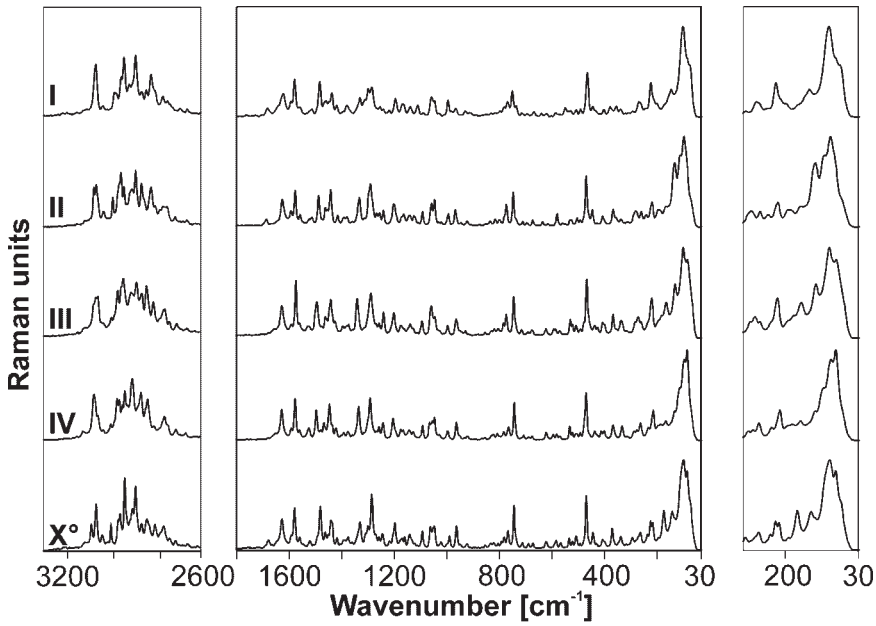

Figure 5. FT-Raman-spectra of APZ forms I, II, III, IV, and X°; right side: enlarged window of the low frequency region.

(<200 cm^{-1}) reflecting the different crystal structures (lattice) of the polymorphs. Other apparent differences concern the range of the CH_2 stretch vibrations of the aliphatic groups (3000–2800 cm^{-1}).

The FT-IR spectra were prepared and recorded on a ZnSe-disk (Fig. 6). Prominent differences in the solid MIR spectra can be found in the region of the (N–H) stretching vibrations of the amide, the regions of the (C–H) stretching and deformation vibrations of the alkyl and aromatic groups, as well as the asymmetric stretch vibrations of the aromatic ether function around 1300 cm^{-1}, which is displayed in an extra window in Figure 6. The

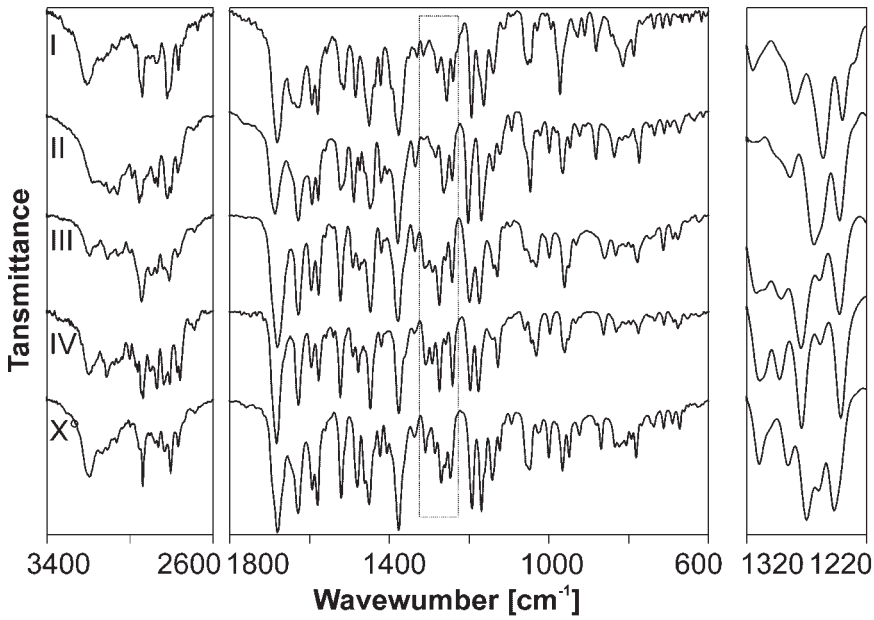

Figure 6. FT-IR-spectra of APZ forms I, II, III, IV, and X°. (Aryl□O) stretch vibration range (1320–1220 cm^{-1}) is enlarged in the right window.

frequencies of some characteristic bands are listed in Table 1.

X-Ray Powder Diffractometry

An overlay of the experimental and calculated powder patterns of the APZ modifications is given in Figure 7. The powder diffractograms allow a clear and fast identification of the APZ polymorphs, especially by the peaks between 2° and 25° 2θ (form I: 10.18°, 13.86°, 18.17°, 19.08°, and 20.75° 2θ; form II: 7.49°, 7.92°, 13.28°, 22.42°, and 23.98° 2θ; form III: 4.76°, 9.54°, 14.35°, 16.93°, and 22.07 2θ; form IV: 2.88°, 5.79°, 8.71°, 11.63°, and 23.39° 2θ; and form X°: 5.33°, 9.94°, 12.55°, 21.77°, and 22.21° 2θ). Due to the typical tabular crystal habit of the forms, relative intensities can strongly depend on sample preparation (preferred orientation effect).

Single Crystal Structure Analysis

The single crystal structures of the five APZ polymorphs were determined at 20°C, and the corresponding crystallographic data are given in Table 2. Form III and IV crystallize in the triclinic crystal system (space group $P\bar{1}$) with two independent molecules. Modifications I and X° are monoclinic ($P2_1$), and form II is orthorhombic ($Pna2_1$). The crystal structures of the polymorphs I, II, IV, and X° are described here for the first time. There was a previous structure determination of form III,[5] and lattice parameters for form X° have been reported recently in a patent application.[7]

Molecular Geometry

The APZ molecule adopts different conformations in the five investigated solid state modifications. Figure 8a shows an overlay of the four APZ conformers present in the triclinic modifications III and IV. A similar overlay for the other three polymorphs is shown in Figure 8b. The torsion angles of the seven freely rotatable bonds and puckering parameters of the terminal ring of the dihydrocarbostyril moiety are given in Table 3 for all five forms. In forms III and IV, there are small, but significant variations (biggest difference 16.4°, involving the C41–C42–C43–C44 torsion angle). However, the conformers of form III differ from the conformers of form IV in the pucker of the saturated part of their dihydrocarbostyril moiety (see Fig. 8a). As a unique feature distinguishing form I from all other APZ modifications, its aliphatic butoxy chain contains two *cis* arrange-

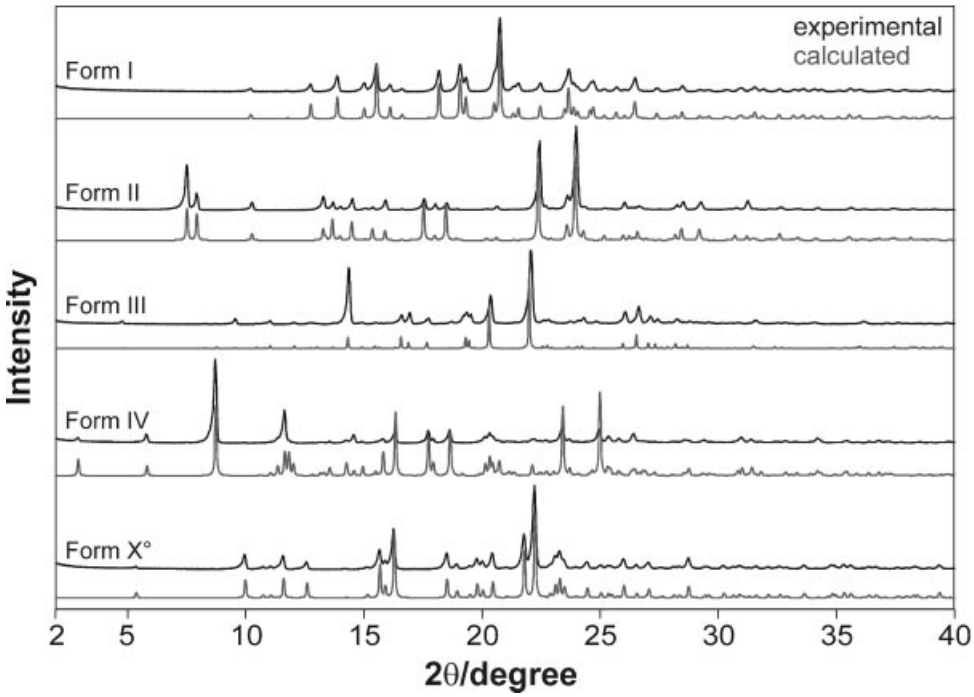

Figure 7. Overlay of experimental versus calculated X-ray powder diffraction patterns of the APZ modifications (recorded at room temperature).

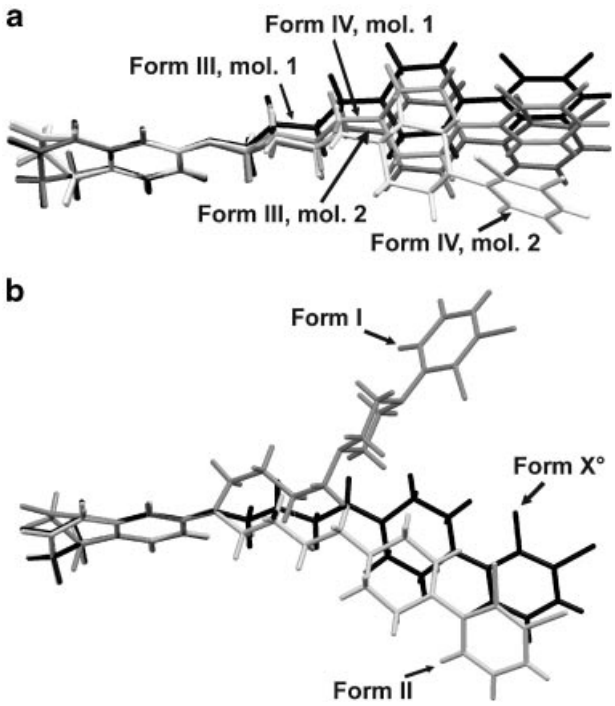

Figure 8. Overlay of the molecules in different APZ polymorphs demonstrating their conformational differences: (a) the two independent molecules of forms III and IV, respectively, (b) conformers of forms I, II, and X°.

ments (vs. all-*trans* for the other conformers, Fig. 8b). This unusual geometry is indicated by the torsion angles N1–C13–C14–C15 and C14–C15–C16–O17. Furthermore, the largest conformational difference between polymorphs I and II and the remaining modifications/conformers is found along the O17–C18 bond, which is associated with a distinctly bent geometry of the APZ molecule of forms I and II. Similar to the triclinic forms, two distinct puckering modes of the dihydrocarbostyril moiety are observed for form I on the one hand and forms II and X° on the other.

Hydrogen Bonding

A common feature of all five structures is the presence of strong N–H···O hydrogen bonds between the amido groups of two adjacent APZ molecules. These interactions result in either of two supramolecular synthons, a catemer (graph set C(4)[24–26]) in forms I, II and X°, and a di-amido $R_2^2(8)$ dimer in polymorphs III and IV. There are two independent, centrosymmetric dimers in form III, while the dimer of modification IV links two crystallographically independent and conformationally distinct APZ molecules. Additionally, similar H-bonded dimeric units are present in three solvated crystal forms of APZ.[12] Thus, the intermolecular organization of all forms is dominated by the self-complementary hydrogen-bonding capacity of the amido group.

A search of the Cambridge Structure Database (CSD)[27] for molecules containing the dihydrocarbostyril moiety resulted in 27 hits of unsolvated structures. Further analysis of strong hydrogen bonds has revealed that in 23 of these cases the characteristic self-complementary hydrogen bonding capabilities of the cyclic amide result in a dimeric arrangement.[28] By contrast, there is just one structure with a catemer (CSD refcode: ZIYROO[29]). The other three dihydrocarbostyril ring containing structures in the CSD show alternative hydrogen bond motifs invoked by the presence of additional strong acceptor and donor groups.

Form III and Form IV

Differences in the packing of these two triclinic forms are associated with the slightly different conformations of the APZ molecule discussed above (see Tab. 3). In form III the molecules adopt a corrugated sheet like arrangement (Fig. 9), while the corresponding sheets of form IV are planar. The latter aggregation mode appears to enable a somewhat closer packing of molecules as witnessed by the higher calculated density of the form IV, which is also thermodynamically slightly more stable. Additional weak interactions of the C–H···O and C–H···Cl types can be identified (see Hirshfeld analysis below). Table 4 gives the geometrical parameters of all strong and weak interactions present in the polymorphs of APZ.

Forms I, II, and X°

Each N–H···O catemer (Fig. 10) contains a 2_1 screw axis. The catemers propagate along the [0 1 0] direction in forms I and X° and along the [0 0 1] direction in form II. Packing diagrams of forms X°, I, and II are depicted in Figure 11, and each structure is viewed parallel to the 2_1 axis of its H-bonded catemer. In forms X° and I, neighboring catemers are related by translation symmetry and additional 2_1 axes. By contrast, neighboring catemers in modification II are related by two sets of glide planes which both lie parallel to the 2_1 axis of the catemer. Thus, a distinct zigzag arrangement of catemeric units is

Table 3. Selected Geometrical Parameters Characterizing the Conformation of the APZ Molecules in Polymorphs I, II, III ($Z' = 2$), IV ($Z' = 2$) and X°

Modification	I	II	III	IV	X°
Torsion angle (°)					
C3–N4–C7–C12	19.6 (6)	21.1 (13)	18.8 (12)	16.1 (4)	14.9 (4)
C31–N32–C35–C40	—	—	21.4 (11)	17.1 (5)	—
C2–N1–C13–C14	−71.1 (6)	−77.4 (11)	−70.5 (8)	−71.4 (3)	−80.2 (4)
C30–N29–C41–C42			−79.0 (10)	−67.4 (4)	
N1–C13–C14–C15	−60.2 (7)	−178.0 (9)	−172.9 (7)	−169.4 (2)	170.6 (3)
N29–C41–C42–C43			−174.2 (9)	179.6 (3)	
C13–C14–C15–C16	−174.7 (6)	173.3 (10)	175.9 (7)	176.5 (3)	169.6 (3)
C41–C42–C43–C44			161.8 (10)	178.2 (3)	
C14–C15–C16–O17	63.2 (11)	178.9 (9)	178.9 (7)	179.6 (2)	174.4 (3)
C42–C43–C44–O45			−177.5 (8)	175.2 (3)	
C15–C16–O17–C18	173.7 (6)	−176.3 (10)	166.0 (7)	176.7 (2)	178.9 (3)
C43–C44–O45–C46			179.6 (8)	−175.3 (3)	
C16–O17–C18–C23	76.4 (8)	−44.1 (14)	2.3 (11)	−5.4 (4)	−6.5 (5)
C44–O45–C46–C51	—	—	2.3 (12)	1.3 (5)	—
C16–O17–C18–C19	−105.1 (7)	140.3 (10)	−175.8 (7)	175.7 (3)	173.1 (3)
C44–O45–C46–C47	—	—	179.0 (8)	−178.3 (3)	—
Deviation (in Å) of atoms C25 (C53), C26 (C54), and O28 (O56) from the plane of the phenyl ring C18–C23 (C46–C51)					
C25	0.355 (7)	−0.476 (16)	0.218 (15)	−0.281 (6)	0.406 (6)
C53			−0.200 (14)	−0.406 (6)	
C26	0.745 (8)	−0.781 (17)	0.577 (16)	−0.545 (6)	0.782 (6)
C54			−0.615 (15)	−0.680 (7)	
O28	0.413 (9)	−0.562 (19)	0.169 (18)	−0.351 (7)	0.458 (7)
O56			−0.095 (16)	−0.534 (7)	

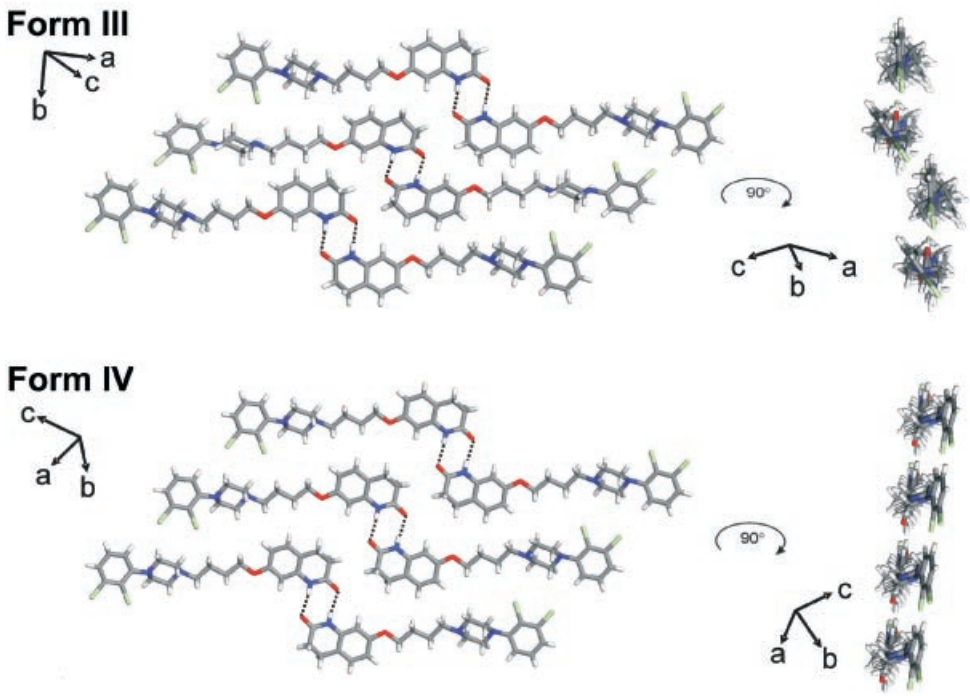

Figure 9. Comparison of the molecular packing of the APZ polymorphs (III and IV) forming dimers.

Table 4. Geometrical Parameters for Intermolecular Interactions in APZ[a] Modifications

Form	Interaction	D (X–H)	d Å	D Å	θ°
Form I	N(24)–H···O(28)	0.86	2.05	2.88	160
	C(19)–H···O(28)	0.93	2.58	3.31	136
	C(3)–H···Cl(1)	0.97	2.91	3.73	144
	C(15)–H···π	0.97	2.96	3.77	142
	C(27)–H···π	0.97	2.78	3.58	140
Form II	N(24)–H···O(28)	0.86	2.01	2.85	165
	C(3)–H···O(28)	0.97	2.69	3.63	165
	C(19)–H···O(28)	0.93	2.69	3.37	131
	C(27)–H···O(17)	0.97	2.71	3.55	146
Form III	N(24)–H···O(28)	0.86	2.01	2.87	172
	N(52)–H···O(56)	0.86	2.04	2.87	164
	C(22)–H···O(56)	0.93	2.63	3.48	153
	C(26)–H···O(56)	0.97	2.60	3.56	176
	C(54)–H···O(28)	0.97	2.71	3.67	172
	C(31)–H···Cl(2)	0.97	2.89	3.66	136
	C(38)–H···Cl(2)	0.93	2.91	3.84	177
Form IV	N(24)–H···O(56)	0.86	2.09	2.93	165
	N(52)–H···O(28)	0.86	2.09	2.93	165
	C(5)–H···O(56)	0.97	2.64	3.41	136
	C(16)–H···O(56)	0.97	2.70	3.58	151
	C(3)–H···Cl(2)	0.97	2.94	3.70	136
	C(30)–H···Cl(3)	0.97	2.91	3.84	162
	C(44)–H···Cl(4)	0.97	2.94	3.64	130
Form X°	N(24)–H···O(28)	0.86	2.06	2.89	161
	C(11)–H···O(28)	0.93	2.68	3.45	141
	C(19)–H···O(28)	0.93	2.63	3.35	134
	C(12)–H···Cl(2)	0.93	2.87	3.62	139
	C(14)–H···π	0.97	2.87	3.81	164
	C(27)–H···π	0.97	2.76	3.56	139

[a]Cut-off: sum of van der Waals radii.

present in polymorph II. A comparison of the densities computed for forms I and X° reveals that the latter polymorph, where the APZ molecule is elongated rather than bent, packs more efficiently and also provides a possible explanation for the higher stability of form X°.

APZ molecules are additionally interlinked by weak C–H···O, C–H···Cl or C–H···π interactions (for geometrical details see Table 4 and Hirshfeld surface analysis below).

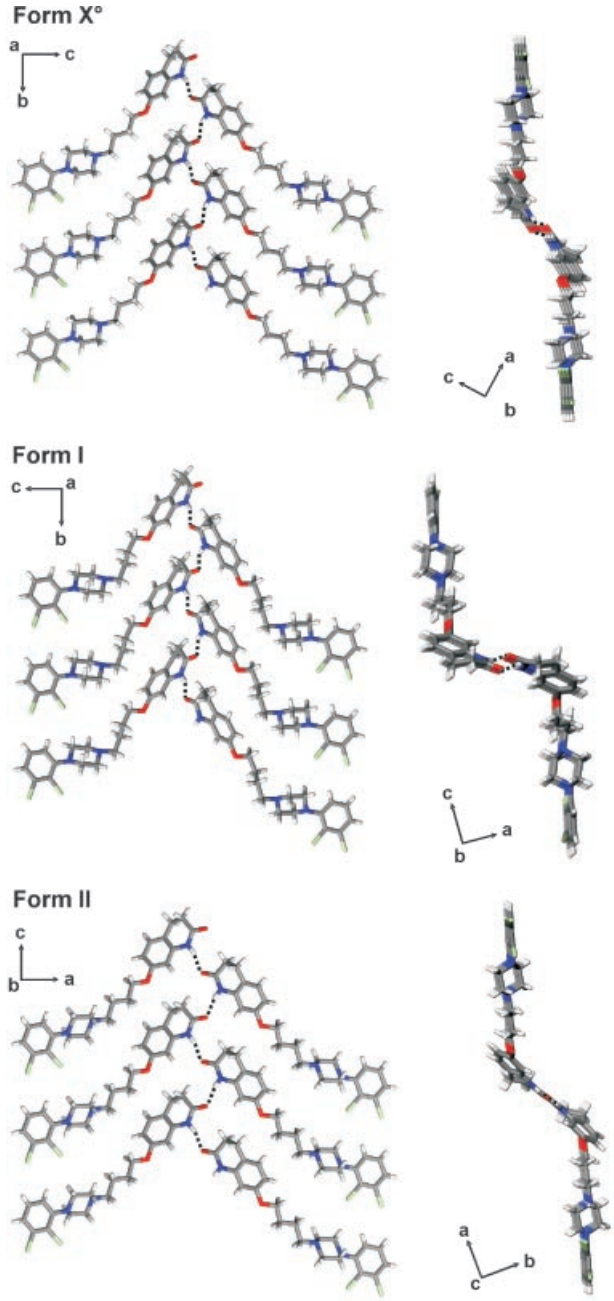

Figure 10. Motif based on strong hydrogen bonds (catemeric chains) in forms X°, I and II of APZ (right: view along 2_1 screw axis).

Hirshfeld 2D Fingerprint Plot

Hirshfeld surfaces are constructed by partitioning space within a crystal structure into regions where the electron density from a sum of spherical atoms dominates over the sum of the electron density of the crystal.[30] Hirshfeld surfaces were constructed with the program *Crystal Explorer*.[31] From the 2D fingerprint plots we can gain information of the overall packing characteristics. It is a plot of d_e against d_i, where d_e is the distance from the surface to the nearest nucleus exterior and d_i interior of the surface. A comparison of the two 2D fingerprint plots[32] for all polymorphs is given in Figure 12. For the two triclinic $Z' = 2$ polymorphs, there is a plot for each conformer and a combined diagram. A major difference between

 DOI 10.1002/jps

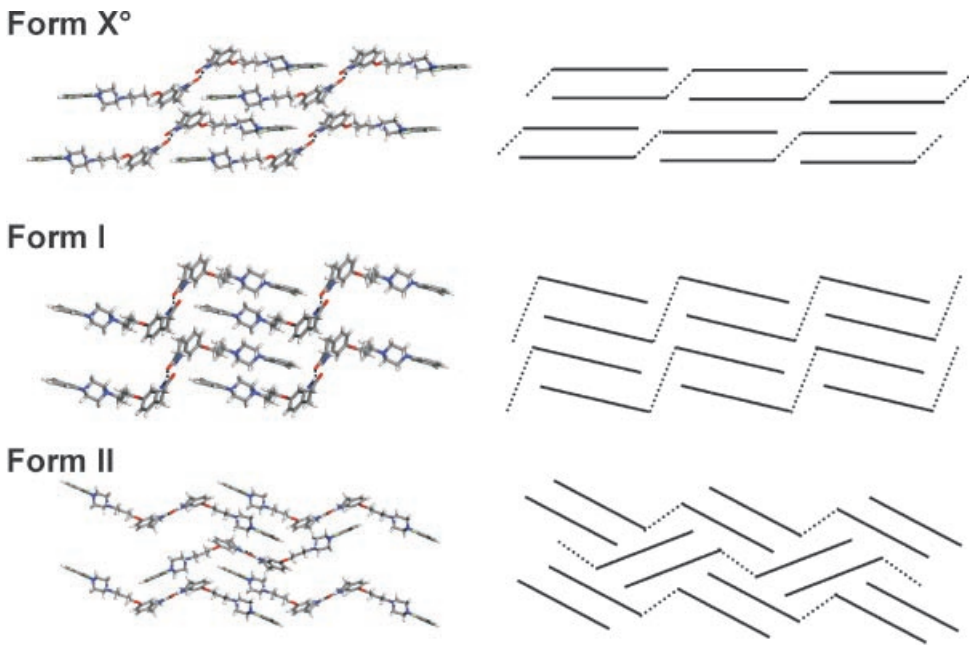

Figure 11. Packing of APZ forms X°, I, and II. Form X° and form I along the *b*-axis, form II along the *c*-axis. Left: only catemeric units along the screw axis are shown for clarity; right schematic drawings (APZ molecule reduced to lines, dotted lines correspond to the N–H···O H-bonds).

the plots of forms III and IV can be seen in the upper right area. It indicates significantly longer interactions and therefore less efficient packing in polymorph III compared with the denser form IV. For clarity, only the three shortest hydrogen bonds/interactions (appearing as spikes; N–H···O interactions labeled with (1) and (2), C–H···Cl with (3)) are marked. The very sharp spikes indicate that the associated angles are close to 180°. Form III shows stronger hydrogen bonds involving only one type of conformer (through an inversion center). By contrast, the hydrogen bonding in form IV involves both conformers of the asymmetric unit. The shortest C–H···Cl hydrogen in form III contact occurs between distinct conformers and in form IV between molecules exhibiting a common conformation. Characteristic wings (marked 4a and 4b in Fig. 12) in the 2D fingerprint plots of the two monoclinic forms (I and X°) indicate C–H···π ($d_e = 1.15$ Å–$d_i = 2.0$ Å and $d_e = 2.0$ Å–$d_i = 1.15$ Å) interactions. These are present in addition to the N–H···O (1), weak C–H···O (not marked in the plots) and C–H···Cl (3) contacts. By, contrast, such wings are absent in the plot of form II as a result of weaker C–H···π interactions. On the other hand, the strong hydrogen bond in form II is slightly shorter than in the two monoclinic polymorphs. Polymorph X° has more weak interactions (cut-off parameter: sum of the van der Waals radii) than forms I and II. The C–H···Cl interactions of form II occur at considerably higher d_e/d_i values and are therefore not listed in the Table 4.

CONCLUSIONS

Five phase pure polymorphs of APZ, verified by their single crystal structures, could be reproduced and comprehensively characterized. APZ is an example of conformational polymorphism,[8–10] which can be expected from its molecular features. The obtained thermochemical data and solvent mediated experiments allowed us to assess the complex thermodynamic relationships of all polymorphs and to construct a semi-schematic energy/temperature diagram. This analysis indicates two monotropic and at least six enantiotropic relationships with transition points above room temperature. The relation of the form X° to the forms III and II could not be clarified unequivocally, because the melting point of X° is not measurable. Nonetheless, the result shows that form X° is the stable polymorph in the temperature range from absolute zero to about 62°C. In a narrow

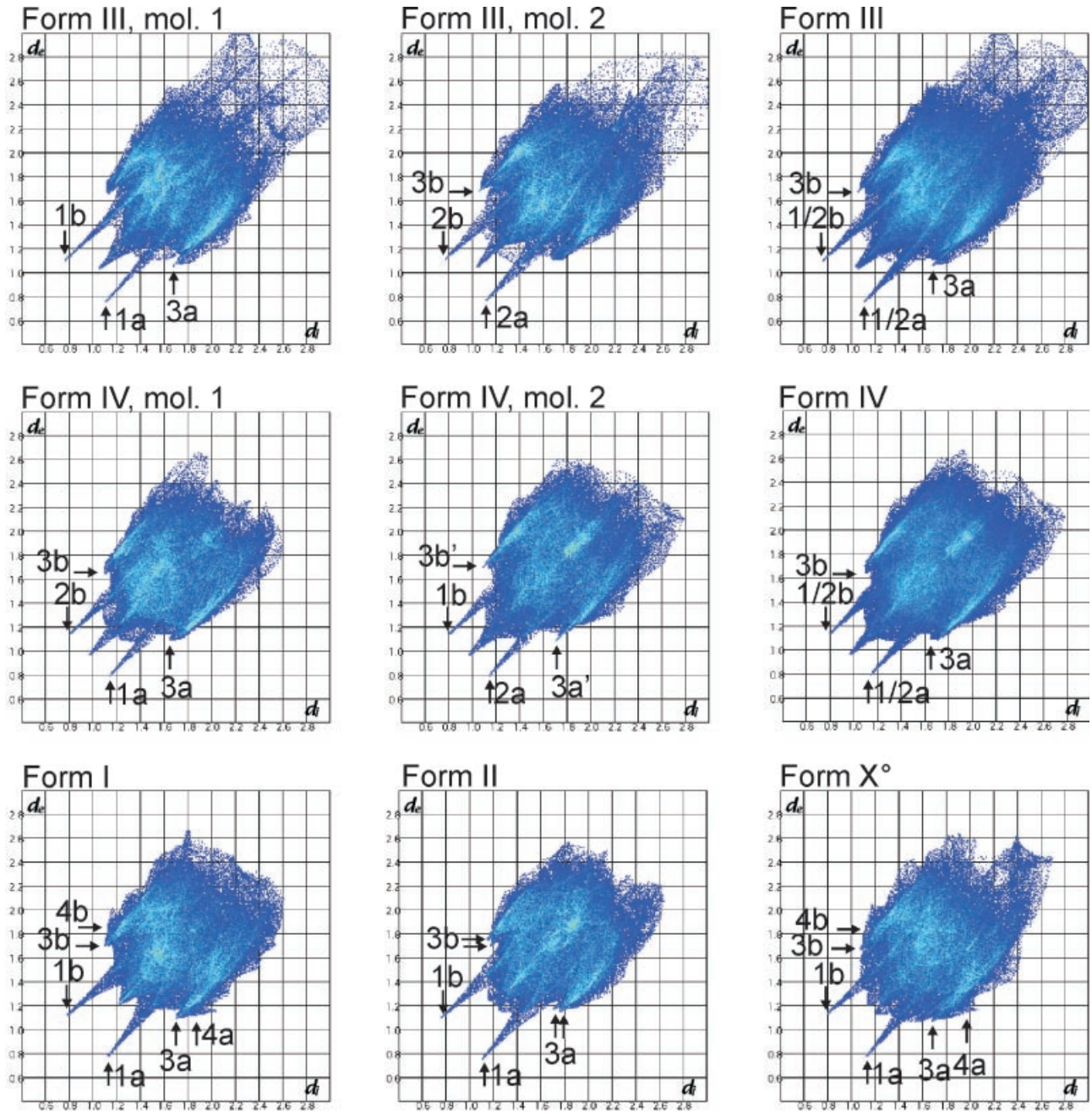

Figure 12. 2D fingerprint plots for APZ polymorphs. d_e and d_i are the distances to the nearest atom center exterior and interior to the surface. N–H···O (1 and 2), C–H···Cl (3), and C–H···π (4); acceptor (a), donor (b).

temperature window (~15°C) between about 62 and 77°C, form II becomes more stable and at higher temperature form I ($T_{fus} = 149.1$°C) represents the polymorph with the highest thermodynamic stability. The forms III and IV are metastable in the entire temperature range. A specific and important characteristic of this polymorphic system is the high kinetic stability of all metastable forms at room temperature, except for form I which transforms on storage within 6 months. Forms II, III, and IV do not change within a year. Thus, these three kinetically highly stable forms are also suitable for the use in pharmaceutical solid dosage forms. However, note that not all forms can be produced easily with high phase purity. Form IV in particular was

often found to crystallize concomitantly with other forms.

Furthermore, we conclude from our investigations that the "type 2" crystals of APZ described in a conference proceeding by Aoki et al.[5] do not represent a pure phase. The reported preparation method, namely annealing "type 1" crystals (phase pure form III) at 130–140°C for 15 h, resulted in form I. Moreover, the XRPD pattern in this publication matches that of form X°. Since our results indicate clearly that form I transforms to form X° under mechanical treatment, we assume that this transformation happened during the sample preparation of that study. Finally the APZ example teaches us that a given drug compound can exist in a considerable number of polymorphs which satisfy the requirement for the successful development of a solid dosage form with respect to their phase stability. This statement is affirmed by the fact that the product is marketed already with the metastable form III.

SUPPORTING INFORMATION AVAILABLE

Electronic Supplementary Information (ESI) available: light photomicrographs, thermal ellipsoid plots, hydrogen bond motifs, and comparison of the packing of the two triclinic APZ modifications. This information is available free of charge via the Internet at http://www.interscience.wiley.com/. The crystallographic data of the forms I, II, III, IV, and X° have been deposited with the Cambridge Crystallographic Data Centre, CCDC Nos. 690583 (I), 690584 (II), 690585 (III), 690586 (IV), 690587 (X°).

ACKNOWLEDGMENTS

The authors gratefully acknowledge Fa. Sandoz GmbH for financial support as well as for the supply of aripiprazole and Dr. R.K.R. Jetti for his assistance in the crystal structure refinements in the early stage of the project.

REFERENCES

1. Green B. 2004. Focus on aripiprazole. Curr Med Res Opin 20:207–213.
2. Otsuka Pharmaceutical Co. 2003. WO 2003/026659 A1.
3. Teva Pharmaceutical Industries Ltd. and Teva Pharmaceuticals. 2005. WO 2005/058835 A2.
4. Selection of recent aripiprazole patent applications: (a) Hetero Drugs Limited. 2004. WO 2004/083183 A1. (b) Cadila Healthcare Limited. 2004. WO 2004/106322 A2. (c) Matrix Laboratories Ltd. 2004. IN CH00272 A. (d) Hetero Drugs Limited. 2005. WO 2005/009990 A1. (e) Beijing Dezhong Wangquan Medicine Technology Development Co. 2005. CN 1676517 A. (f) Venkataraman S, Reddy PP, Satyanarayana B, Rangareddy T. 2005. US 2005/277650 A1. (g) Shanghai Institute of Pharmaceutical Industry. 2006. WO 2006/012237 A2. (h) Matrix Laboratories Ltd. 2006. WO 2006/030446 A1. (i) Chongqing Pharmaceutical Research Institute Co. 2006. CN 1760183 A. (h) Synthon BV. 2006. WO2006/053780 A1. (j) Chemagis Ltd. 2006. WO 2006/077584 A2. (k) Sandoz A-G. 2006. WO 2006/079548 A1. (l) Synthon BV. 2006. WO 2006/097343 A1. (m) Synthon BV. 2006. WO 2006/053780 A1. (n) Teva Pharmaceutical Industries Ltd. and Teva Pharmaceuticals. 2007. WO2007/041414 A1. (o) Eisen-Nevo H, Pavlov Z. 2007. US 2007/161794 A1. (p) Shanghai Institute of Pharmaceutical Industry. 2007. CN 17727387 A. (q) Chongqing Pharmaceutical Research Institute Co. 2007. CN 1896063 A.
5. Aoki B, Bando T, Kobayashi N. 1996. Study on Crystal Transformation of Aripiprazol [The fourth Japan-Korea Symposium on Separation Technology].
6. Tessler L, Goldberg I. 2006. Crystal structures of aripiprazole, a new anti-psychotic drug, and of its inclusion compounds with methanol, ethanol and water. J Incl Phenom Macro 55:255–261.
7. Medichem SA. 2007. WO 2007/004061A1.
8. a) Bernstein J, Hagler AT. 1978. Conformational polymorphism. The Influence of crystal structure on molecular conformation. J Am Chem Soc 100: 673–681.8.;
   b) Bernstein J. 2002. Polymorphism in molecular crystals. Oxford: Oxford University Press. p 410.
9. Nangia A. 2008. Conformational polymorphism in organic crystals. Acc Chem Res 41:595–604.
10. Griesser UJ, Jetti R, Haddow MF, Brehmer T, Harris RK. 2008. Conformational polymorphism in oxybuprocaine hydrochloride. Cryst Growth Des 8:44–56.
11. Braun DE, Gelbrich T, Kahlenberg V, Laus G, Wieser J, Griesser UJ. Packing polymorphism of a conformationally flexible molecule (aprepitant). New J Chem DOI: 10.1039/b805438j.
12. Braun DE, Gelbrich T, Kahlenberg V, Tessadri R, Wieser J, Griesser UJ. Unpublished results (submitted to Cryst Growth Des).
13. Colthup NB, Daly LH, Wiberley SE. Introduction to infrared and Raman spectroscopy. New York: Academic Press. p 547.

14. Farrugia LJ. 1999. WinGX suite for small-molecule single-crystal crystallography. J Appl Cryst 32: 837–838.
15. Altomare A, Burla MC, Camalli M, Cascarano GL, Giacovazzo C, Guagliardi A, Moliterni AGG, Polidori G, Spagna R. 1999. SIR97: A new tool for crystal structure determination and refinement. J Appl Cryst 32:115–119.
16. Sheldrick GM. 2008. A short history of SHELX. Acta Crystallogr A64:112–122.
17. Burger A, Ramberger R. 1979. On the polymorphism of pharmaceuticals and other molecular crystals. I. Theory of thermodynamic rules. Mikrochim Acta 2:259–271.
18. Burger A, Ramberger R. 1979. On the polymorphism of pharmaceuticals and other molecular crystals. II. Applicability of thermodynamic rules. Mikrochim Acta 2:273–316.
19. Grunenberg A, Henck J-O, Siesler HW. 1996. Theoretical derivation and practical application of energy/temperature diagrams as an instrument in preformulation studies of polymorphic drug substances. Int J Pharm 129:147–158.
20. Kitaigorodsky AI. 1973. Molecular crystals and molecules. New York, London: Academic Press.
21. Yu L. 1995. Inferring thermodynamic stability relationship of polymorphs from melting data. J Pharm Sci 84:966–974.
22. Griesser UJ, Weigand D, Rollinger JM, Haddow M, Gstrein E. 2004. The crystal polymorphs of metazachlor. J Therm Anal Calorim 77:511–522.
23. Henck J-O. 1995. Konformationspolymorphie n-butylsubstituierter Arzneistoffe. Innsbruck: Thesis, p 41.
24. Bernstein J, Davis RE, Shimoni L, Chang N-L. 1995. Patterns in hydrogen bonding: Functionality and graph set analysis in crystals. Angew Chem Int Ed 34:1555–1573.
25. Etter MC, MacDonald JC, Bernstein J. 1990. Graph-set analysis of hydrogen-bond patterns in organic crystals. Acta Crystallogr B46:256–262.
26. Etter MC. 1990. Encoding and decoding hydrogen-bond patterns of organic compounds. Acc Chem Res 23:120–126.
27. All CSD (version 5.28) searches were performed using Conquest version 1.9 (November 2006, 390081 entries) with the following filters used: 3D coordinates determined, not disordered, R-factor less than 10%, no errors, not polymeric and only organics.
28. Allen F, Shields GP, Taylor R, Raithby PR. 1998. Probabilities of formation of bimolecular cyclic hydrogen-bonded motifs in organic crystal structures: A systematic database analysis. Chem Commun 9:1043–1044.
29. Uno T, Ozeki Y, Koga Y, Chu G-N, Okada M, Tamura K, Igawa T, Unemi F, Kido M, Nishi T. 1995. Synthesis of 2(1H)-quinolinone derivatives and their inhibitory activity on the release of 12(S)-hydroxyeicosatetraenoic acid (12-HETE) from platelets. Chem Pharm Bull 43:1724–1733.
30. McKinnon JJ, Spackman MA, Mitchell AS. 2004. Novel tools for visualizing and exploring intermolecular interactions in molecular crystals. Acta Crystallogr B60:627–668.
31. Wolff SK, Grimwood DJ, McKinnon JJ, Jayatilaka D, Spackman MA. 2007. Crystal Explorer, Version 2.0. University of Western Australia. Australia.
32. Spackman MA, McKinnon JJ. 2002. Fingerprinting intermolecular interactions in molecular crystals. CrystEngComm 4:378–392.